We are IntechOpen,
the world's leading publisher of
Open Access books
Built by scientists, for scientists

5,900
Open access books available

146,000
International authors and editors

185M
Downloads

154
Countries delivered to

Our authors are among the

TOP 1%
most cited scientists

12.2%
Contributors from top 500 universities

CLARIVATE ANALYTICS
BOOK CITATION INDEX
INDEXED

WEB OF SCIENCE™

Selection of our books indexed in the Book Citation Index
in Web of Science™ Core Collection (BKCI)

Interested in publishing with us?
Contact book.department@intechopen.com

Fracture Network Connectivity — A Key To Hydraulic Fracturing Effectiveness and Microseismicity Generation

F. Zhang, N. Nagel, B. Lee and M. Sanchez-Nagel

Additional information is available at the end of the chapter

Abstract

In this work, the effect of fracture network connectivity on hydraulic fracturing effectiveness was investigated using a discrete element numerical model. The simulation results show that natural fracture density can significantly affect the hydraulic fracturing effectiveness, which was characterized by either the ratio of stimulated natural fracture area to hydraulic fracture area or the leakoff ratio. The sparse DFN cases showed a flat microseismic distribution zone with few events, while the dense DFN cases showed a complex microseismic map which indicated significant interaction between the hydraulic fracture and natural fractures. Further, it was found that the initial natural fracture aperture affected the hydraulic fracturing effectiveness more for the dense natural fracture case than for the sparse (less dense) case. Overall, this work shows that fracture network connectivity plays a critical role in hydraulic fracturing effectiveness, which, in-turn, affects treating pressures, the created microseismicity and corresponding stimulated volume, and well production.

1. Introduction

The extremely low permeability of the common shale plays means that simple, bi-planar hydraulic fractures (HF) do not create enough surface area to make economic wells and that stimulation of the natural fracture system is critical [1]. Numerous field microseismic data sets have shown that extreme fracture complexity may result from the interaction between a created hydraulic fracture and the pre-existing fracture network [2, 3]. Consequently, operators will often alter the stimulation design, by changing injection rate, viscosity, or other parameters, in order to improve the effectiveness of the stimulation in unconventional shale plays.

However, these design changes offer only a limited control on improving the stimulation of natural fractures because of a lack of understanding of the fundamental characteristics, behavior, and connectivity of the natural fracture network.

The connectivity of the fracture network, for example, determines the overall hydraulic diffusivity of the formation and is a key to the resulting 'complexity' from a hydraulic fracture stimulation. A highly connected fracture network will allow more fluid leakoff into the rock mass and render pressure communication over large distances, whereas a partially or sparsely connected fracture network will favor the propagation of a new hydraulic fracture and may exhibit pressure isolation between very closely spaced hydraulic fractures. The intricacy of fluid flow in fractured formation is mainly due to the complex geometries, patterns, and heterogeneity of the fracture network. The fracture network connectivity, therefore, has been shown to be a critical factor which affects treating pressures, the created microseismicity and corresponding SRV (Stimulated Rock Volume), and production.

Numerous numerical modeling efforts have been conducted in order to understand the process of hydraulic fracture (HF) interaction with a complex natural fracture network [4, 5, 6]. However, relatively few works have focused on understanding the role of natural fracture network connectivity and its impact on the effectiveness of hydraulic fracturing of shale reservoirs and associated microseismicity generation.

In this paper, a discussion of fracture network connectivity and how it is utilized in developing a discrete fracture network (DFN) is presented, which is then incorporated into a discrete element numerical model (DEM). The propagation of a HF in the fractured rock mass was then studied using the DEM, which allowed for fully coupled, hydro-mechanical simulations, including the generation of synthetic microseismicity. Following previous work [7, 8, 9, 10] from the authors on parametric studies to analyze the influence of the mechanical and flow properties of the DFN and matrix on HF propagation, the influence of the DFN fracture network connectivity was analyzed in this work using common stimulation metrics such as SRV. The corresponding microseismic response was also calculated from the simulation results and related to the effective SRV. The results show not only the critical role that the DFN must play in resource evaluations, but also in completion design and stimulation optimization.

2. Fracture network connectivity and DFN realization

Fracture network connectivity is determined by many statistical characteristics, among them, fracture shape, fracture size distribution, fracture density (area of fracture per unit volume), orientation distribution, and aperture size distribution. The combinations of these statistical characteristics that describe the geometrical properties of a DFN define the macro-scale connectivity and directional flow preference of the DFN, and thus, are essential for the fluid transport characterization of an unconventional reservoir.

In this work, focus was placed on the effects of two statistical fracture characteristics, fracture density and initial aperture both individually and in combination, on hydraulic fracturing

effectiveness and microseismicity generation. For the study, a DFN generator was developed that was capable of creating a fracture network that satisfied the assigned input statistical characteristics and allowed for the quantitative variation of network connectivity.

As shown in Figure 1, two DFN configurations were realized, which represent a sparse DFN and a dense DFN, respectively. The sparse DFN had 191 fractures while the dense DFN had 482 fractures, or about 2.5 times more than the sparse DFN. The fractures were created in the common disk shape with a dip angle of 90° but either a 60° or 150° dip direction in order to construct two orthogonal fracture sets. The P10 (the number of fractures along a line divided by the length of the line) for the sparse DFN and dense DFN was 0.079 m^{-1} and 0.28 m^{-1}, respectively. The P32 (the sum of the areas of the fractures contained in a named volume divided by the same volume) for the sparse DFN and dense DFN was 0.031 m^2/m^3 and 0.075 m^2/m^3, respectively.

In addition to DFN density, the effect of the initial DFN aperture was studied by considering two different values of initial aperture for the DFN fractures. In the first case, it was assumed that the initial aperture of the DFN fractures was equal to 0.1 mm. In the second case, it was assumed that the DFN fracture aperture was 1.5 times greater and equal to 0.15 mm.

The goal of this study was to investigate the effects of hydraulic fracturing in shale formations with different levels of DFN connectivity. It was assumed that the DFN fractures were static, meaning that, with the exception of the main hydraulic fracture itself, the process of fracture growth and propagation was not considered within the simulations.
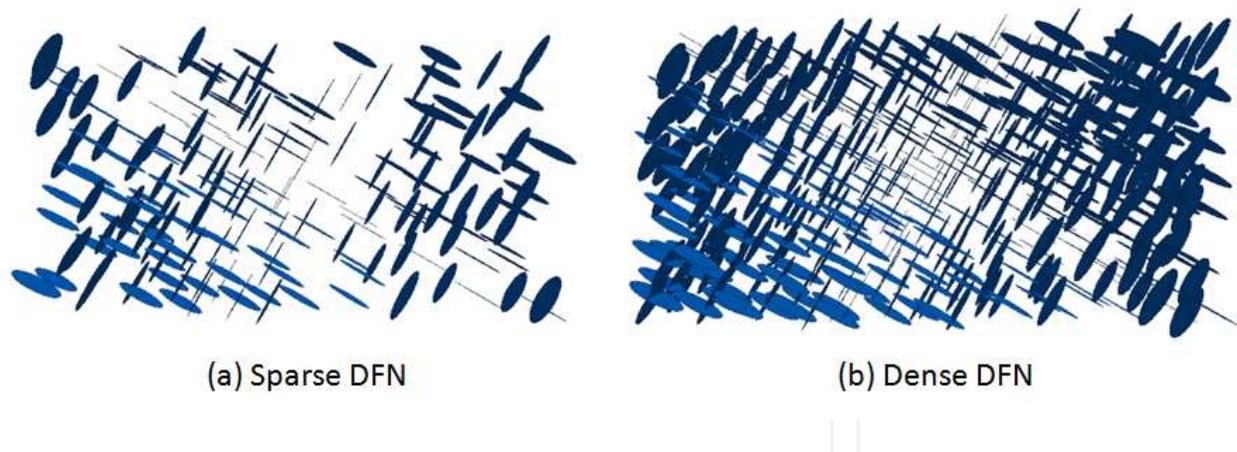

(a) Sparse DFN   (b) Dense DFN

Figure 1. Plan view of two DFN realizations. A) Sparse DFN with 191 fractures; and B) Dense DFN with 482 fractures.

3. Numerical simulations

3.1. *3DEC* hydraulic fracturing modeling capabilities

The numerical code used in the simulations, *3DEC,* is a three dimensional distinct element method for discontinuum modeling [11]. It can simulate the response of discontinuous media,

such as a jointed rock mass, subjected to either static or dynamic loading, which includes the simulation of fluid injection during a hydraulic fracture treatment. *3DEC*'s ability to handle large block displacements makes it amenable to the simulation of hydraulic fracture propagation, fracture opening (both hydraulic fracture and natural fractures), and the rotation of individual blocks leading to fracture connections or pinching. Further, *3DEC* includes the ability to model steady-state or transient-fracture fluid flow, where the flow logic includes a system of flow planes, flow pipes and flow knots. While most of the existing commercial hydraulic fracture simulators are based upon a number of analytical assumptions, or limit the simulated fractures to be smooth, bi-planar cracks, *3DEC* is capable of explicitly modeling the mechanical response of a fracture network to fluid injection as well as the interaction of a created hydraulic fracture (the HF plane needs to be pre-defined) with the existing natural fractures.

3.2. *3DEC* model setup

The *3DEC* simulation domain consisted of two parts: an inner core domain with the population of the DFN and an outer boundary domain, which extended to twice of the size of the core domain in order to minimize boundary effects. To port the created natural fractures to *3DEC*, a procedure was developed to explicitly represent the generated DFN in the geomechanical model. For each DFN fracture, a search was performed to identify those *3DEC* blocks that were intersected by the given fracture. The identified blocks were then cut through into two blocks by the fracture plane. Since the newly created plane between blocks might only have part of its area belonging to the given fracture (if the natural fracture did not fully cut the blocks), different fracture material properties were assigned to the portion of the newly created plane that fell within the geological fractures than to the unfractured portion that fell outside the geological fractures.

Figure 2 shows the core simulation domain discretized by the dense DFN. Individual blocks are shown in variable color, while the plane between two blocks is a possible natural fracture. The size of the inner domain was 400×200×100 m. The directions of the three principal stresses are shown in Figure 2, which are coincident with the three axes x, y and z.

For all the simulations, the maximum horizontal stress (SHmax) was 55 MPa, the minimum horizontal stress (Shmin) was 50 MPa, and the vertical stress (Sv) was 60 MPa. The initial pore pressure was set to 45 MPa. The Young's modulus of the rock mass was set to 30.0 GPa and Poisson's ratio was set to 0.25. The injection point was located in the center of the domain along the predefined hydraulic fracture plane (the plane of y=0), which was parallel to SHmax. The injection rate was 0.05 m^3/s and the fluid viscosity was 0.0015 Pa s. It was assumed that fluid flow only occurred in either the DFN or HF planes and that there was no fluid flow into the rock matrix during the simulations.

3.3. Simulation results

In this study, four simulation cases, consisting of two DFN configurations (i.e., the dense DFN and sparse DFN) and two initial DFN apertures (i.e., 0.1 mm and 0.15 mm) were analyzed.
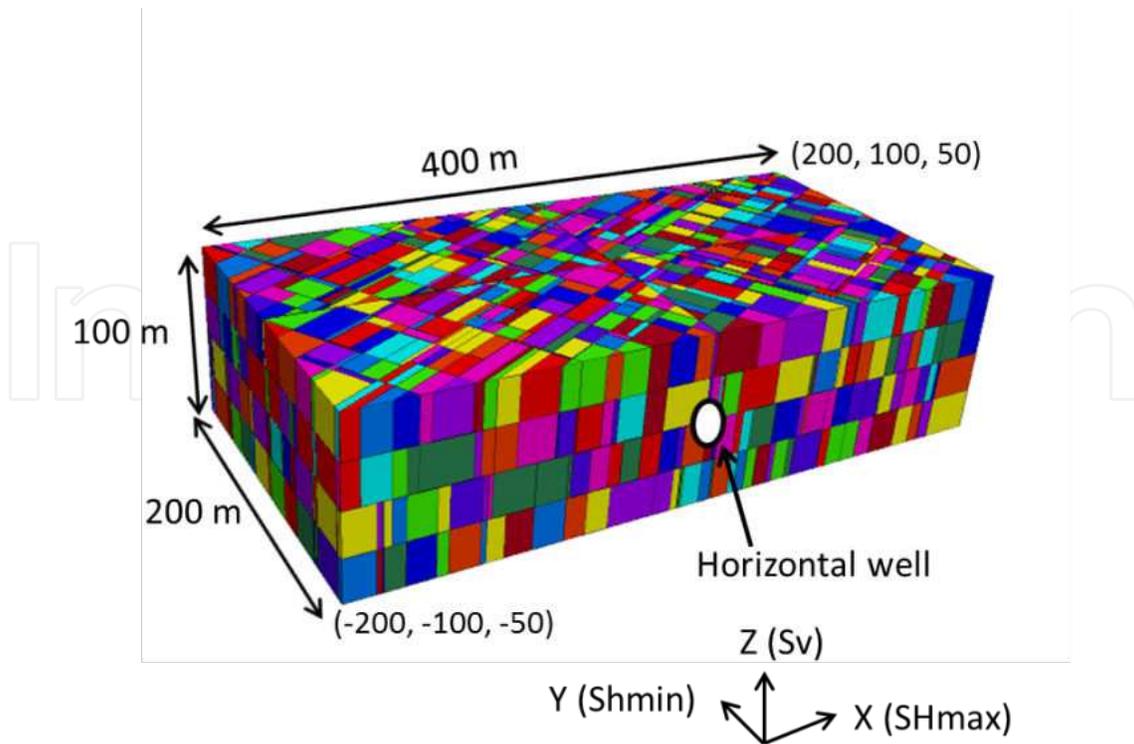
Figure 2. The core domain of the numerical model discretized by the dense DFN. Blocks are distinguished by colors. The plane of y=0 is the HF plane.

Figure 3 shows a plan view of the contours of fracture pressure distribution at the XY plane of z=0 m after 900 s of injection time for the four tests.

The fracture pressure contour plot suggests two major observations. With the same initial DFN aperture, the case with the dense DFN resulted in significantly more stimulated DFN area and less stimulated HF area than the case with the sparse DFN. In addition, with the same DFN configuration, the case with 0.15 mm initial aperture resulted in more stimulated DFN area and less stimulated HF area than the case with 0.1 mm initial aperture. These results are also confirmed by the shorter hydraulic fracture lengths in the dense DFN simulations.

These qualitative conclusions are as expected. Since hydraulic fracturing represents, essentially, the release (injection) of hydraulic energy into the formation, the injected fluid will follow the least resistive path. For the dense DFN, it was easier for fluid to enter the natural fractures than it was for the fluid to propagate a hydraulic fracture.

The synthetic microseismic events during the injection can be approximated based on the magnitude of plastic slip. Figure 4 plots the synthetic microseismic moment magnitudes for the sparse and dense DFN with the same initial aperture (0.1 mm) after 900 s of injection time. The events that clustered based on their spatial and temporal proximity were colored by the occurring time and sized by the microseismic moment magnitude. All events were projected onto the XY plane with z=0 m and the XZ plane with y=0 m (HF plane). Figure 4 shows that the sparse DFN case had fewer microseismic events than the dense DFN case. The complexity of microseismic events for the dense DFN case was consistent with field observations and
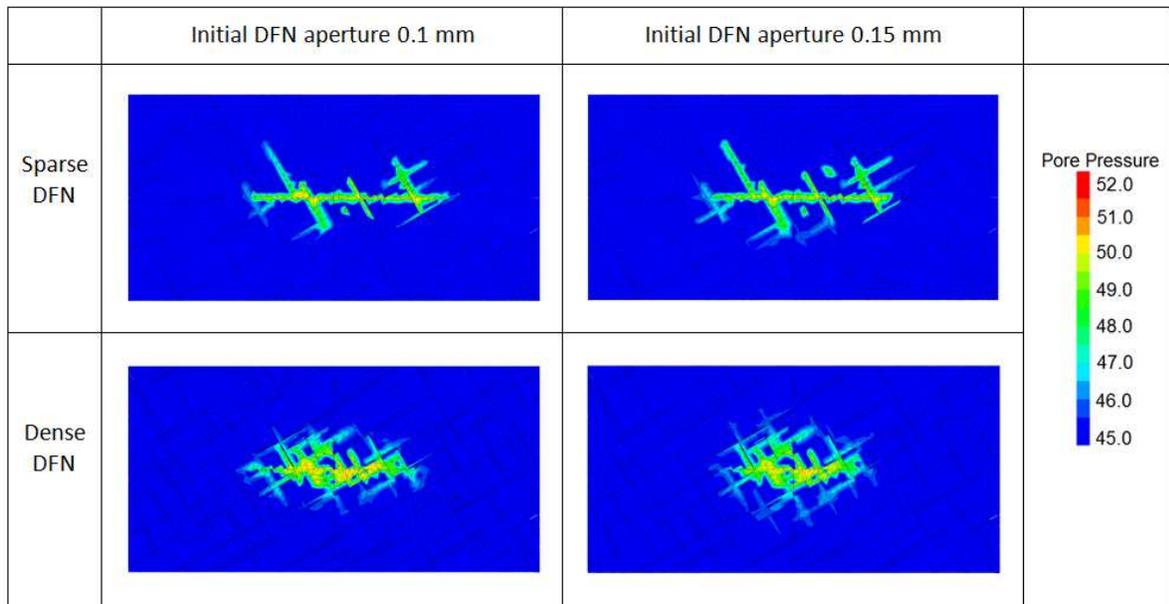
Figure 3. Plan view of contours of fracture pressure distribution at the XY plane of z=0 m after a 900 s injection time for the cases of sparse and dense DFN realizations with two initial DFN apertures.

suggests an intensive interaction between the created hydraulic fracture and the natural fractures.

The two qualitative observations from Figure 3 were further proved quantitatively by tracking the evolution of stimulated DFN area and HF area. As there is no precise criteria for defining the stimulated area, a criteria based on fracture pressure change was employed in this work. The area of the DFN or HF planes having a fracture pressure increase of 0.5 MPa or 1 MPa above the initial fracture pressure was considered as the stimulated area.

Figure 5 shows the quantitative evolution of the stimulated DFN area with a fracture pressure increase greater than 0.5 MPa and 1 MPa for the four cases shown in Figure 3. Figure 5 shows that, with the same DFN configuration, the case with a 0.15 mm initial aperture produced about twice the stimulated DFN area as the case with a 0.1 mm initial aperture. However, with the same initial aperture, the case with the dense DFN produced only slightly more stimulated DFN area than the case with a sparse DFN. Figure 5 also shows that the effect of choosing a different fracture pressure increase threshold to define the stimulated DFN areas is more obvious for the dense DFN case.

Figure 6 plots the evolution of the stimulated HF area with a fracture pressure increase greater than 0.5 MPa and 1 MPa for the four cases shown in Figure 3. Figure 6 shows that, for the sparse DFN configuration, the case with a 0.15 mm initial aperture produced only slightly less stimulated HF area than the case with a 0.1 mm initial aperture, whereas for the dense DFN configuration, there was nearly a 20% reduction in stimulated HF area for the 0.15 mm initial aperture over the 0.1 initial aperture case. Comparing the same initial aperture cases, the cases with the dense DFN produced much less stimulated HF area than the cases with a sparse DFN.
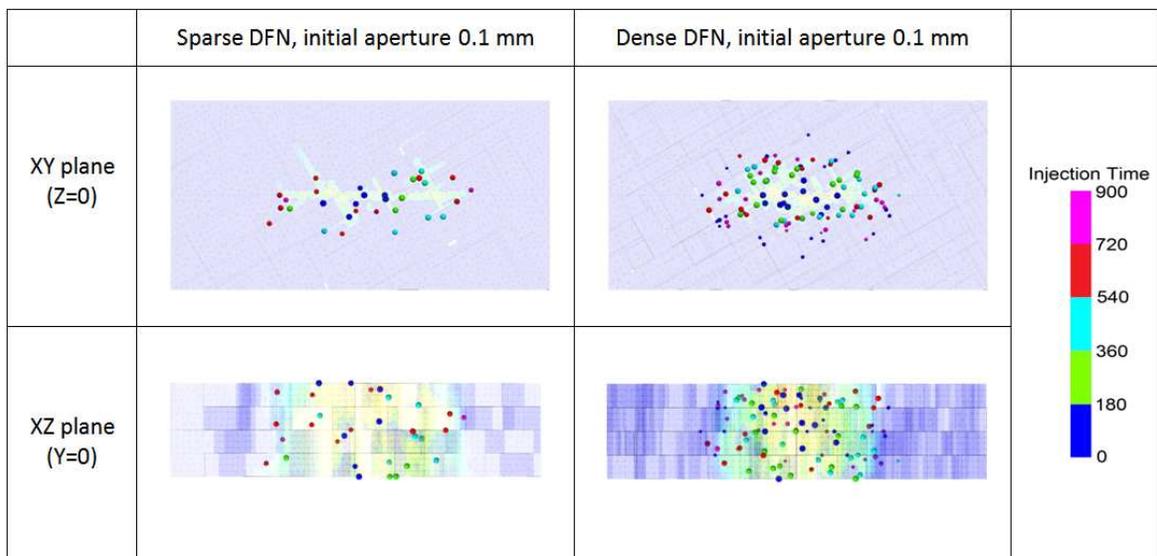
Figure 4. Synthetic microseismic events for the sparse and dense DFN with the same initial aperture 0.1 mm after 900 s of injection time. The synthetic microseismic events are colored by the occurring time and sized by moment magnitude and then projected in the XY plane with z=0 m and the XZ plane with y=0 m (HF plane).
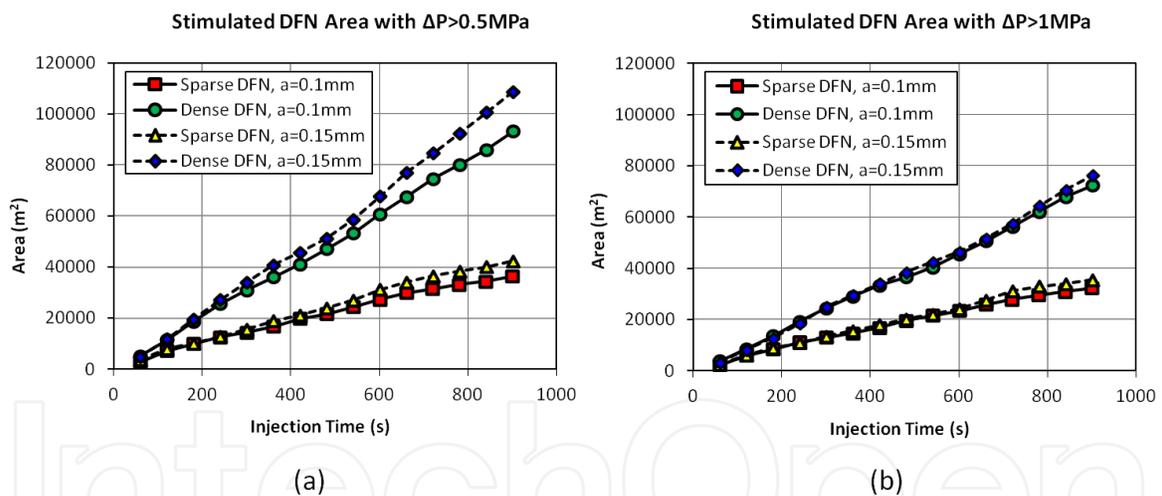

Figure 5. Stimulated DFN area with a fracture pressure increase greater than A) 0.5 MPa and B) 1 MPa for the four cases shown in Figure 3.

Figure 6 also shows that the stimulated HF areas for all four cases using the 0.5 MPa fracture pressure increase criteria were only slightly larger than the cases when using the 1.0 MPa fracture pressure increase criteria.

It may be concluded from the above analysis that, in terms of the stimulated DFN area, the initial DFN aperture is a more sensitive parameter than the DFN density. On the contrary, in terms of the stimulated HF areas, the DFN density seems to be a more sensitive parameter than the initial DFN aperture.
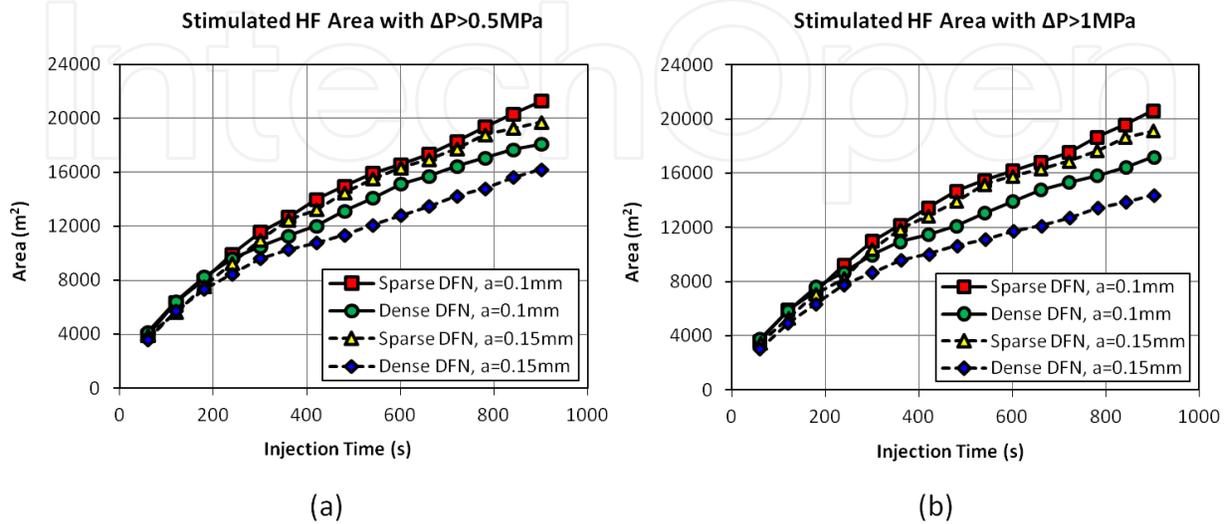
Figure 6. Stimulated HF area with a fracture pressure increase greater than A) 0.5 MPa and B) 1 MPa for the four cases shown in Figure 3.

The overall effect of fracture network connectivity on hydraulic fracturing effectiveness can also be characterized by the ratio of stimulated DFN area to stimulated HF area. Figure 7 plots the ratio of stimulated DFN area to stimulated HF area with a fracture pressure increase of 0.5 MPa and 1 MPa for the four cases shown in Figure 3. It can be seen that a dense DFN created a much higher ratio of stimulated DFN area to stimulated HF area than did a sparse DFN for similar initial apertures. However, the effect of initial DFN aperture was more evident for the dense DFN configuration than for the sparse DFN configuration. Meanwhile, the effect of choosing a different fracture pressure increase threshold for the stimulated areas was more obvious in the dense DFN configuration than for the sparse DFN configuration.

Another parameter to evaluate the overall effect of fracture network connectivity on hydraulic fracturing effectiveness is the leakoff ratio, which is defined as the ratio of fluid volume in the DFN over the total fluid volume injected into the model. Figure 8 shows the leakoff ratio for the four cases shown in Figure 3. Very similar with the analysis for the ratio of stimulated DFN area to stimulated HF area, DFN density is shown to significantly affect the leakoff ratio for both initial aperture cases, while the initial DFN aperture is seen to affect the dense DFN more than the sparse DFN configuration.
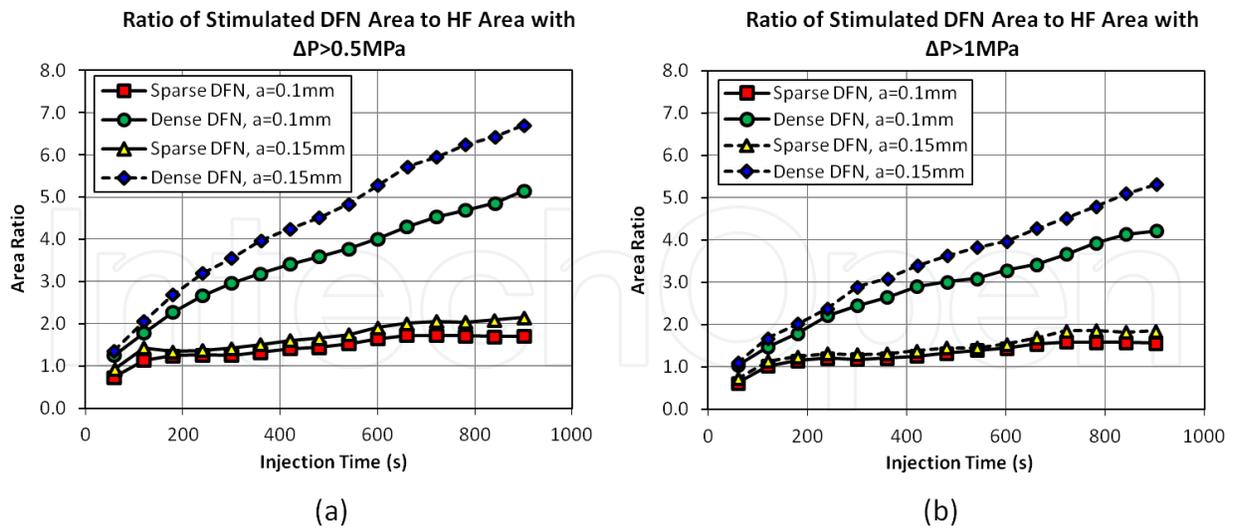
Figure 7. Ratio of stimulated DFN area to stimulated HF area with a fracture pressure increase greater than A) 0.5 MPa and B) 1 MPa for the four cases shown in Figure 3.
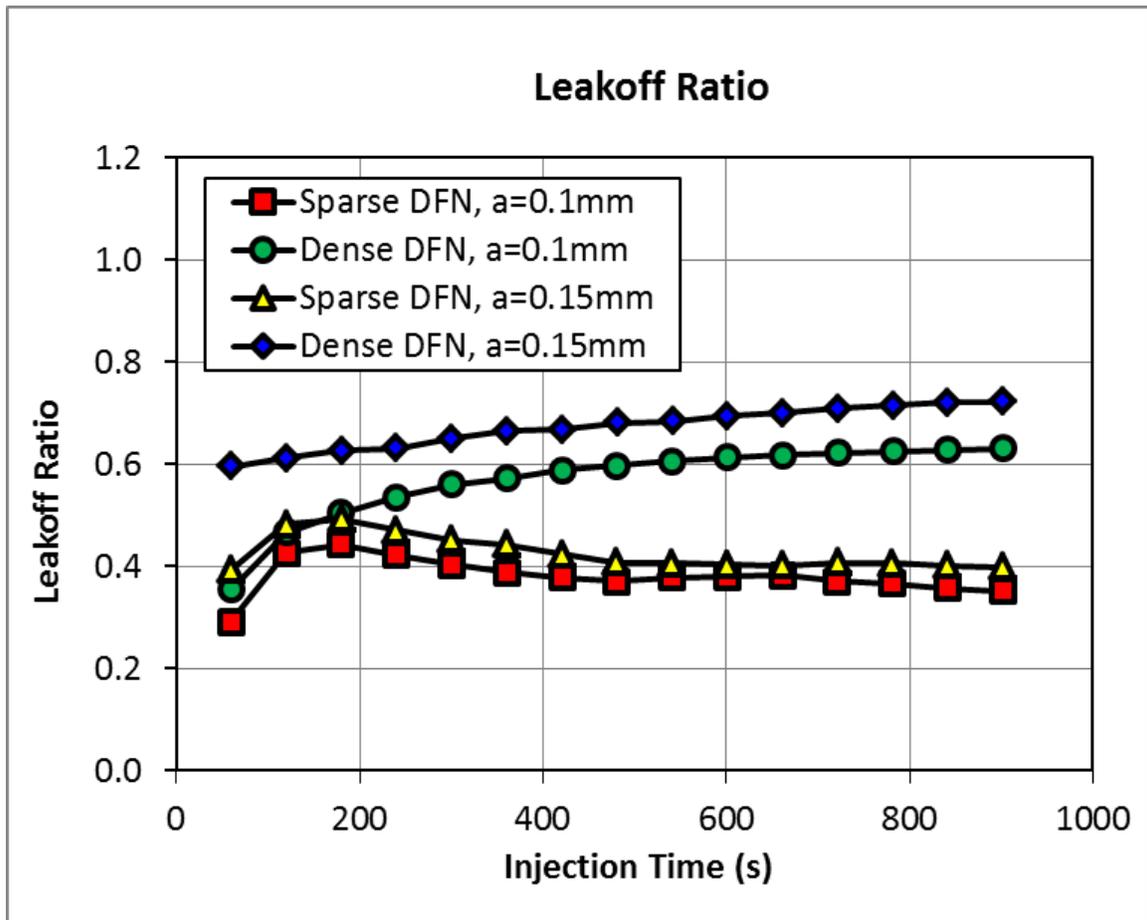

Figure 8. Leakoff ratio for the four cases shown in Figure 3.

Figure 9 and Figure 10 show, separately, the average DFN aperture and average HF aperture for the four cases shown in Figure 3. The average DFN aperture for all cases increased only slightly during the injection, though it is worth mentioning that even though the natural fractures were only slightly opened, the leakoff ratio for the dense DFN cases reached about 50% or more.

Relatively, the sparse DFN case showed a slightly greater increase of average DFN aperture than the dense DFN case with the same initial DFN aperture. As expected, the average HF apertures for all cases were several times larger than the average DFN apertures. In addition, as shown in Figure 9, the sparse DFN case had a much greater increase (more than double) in the average HF aperture than the dense DFN case with the same initial DFN aperture.
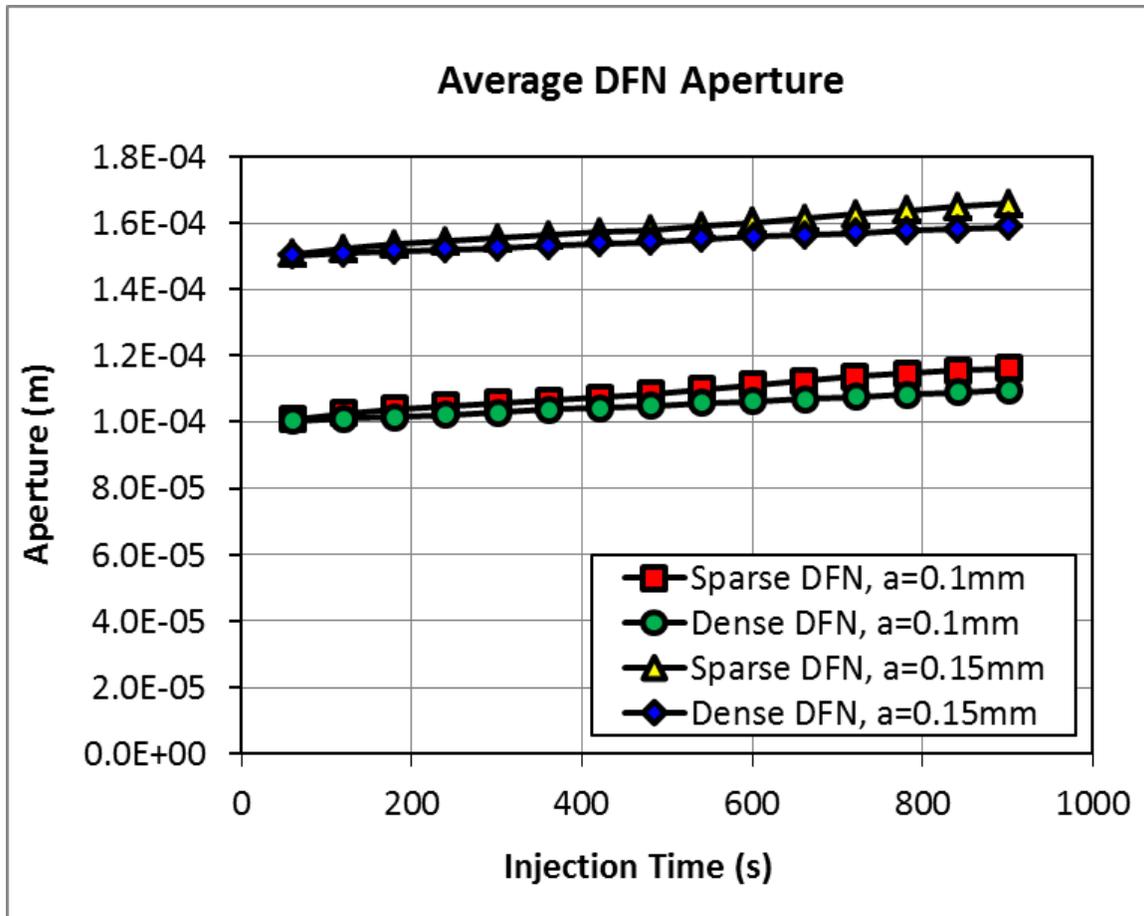

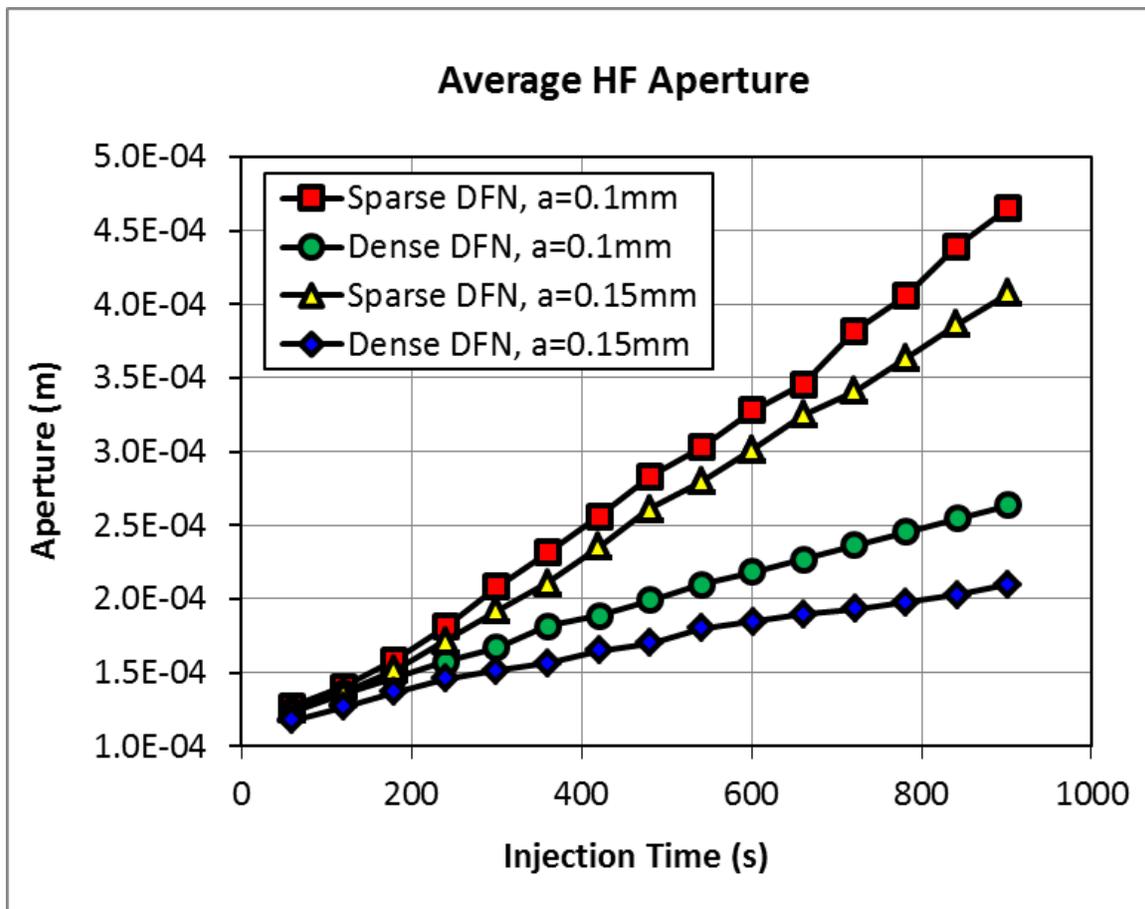**Figure 9.** Average DFN aperture for the four cases shown in Figure 3.

Figure 10. Average HF aperture for the four cases shown in Figure 3.

4. Conclusions

In this work, the effect of fracture network connectivity on hydraulic fracturing effectiveness (extent of stimulation of the natural fractures) was investigated using a discrete element numerical model. Four simulation cases were evaluated using two DFN configurations (i.e., a dense DFN and a sparse DFN) and two initial DFN apertures (i.e., 0.1 mm and 0.15 mm). The main conclusions from this study are summarized in the following points:

• DFN density significantly affected hydraulic fracturing effectiveness, characterized by either the ratio of stimulated DFN area to stimulated HF area or the leakoff ratio, for both initial apertures considered. Further, the initial DFN aperture affected the hydraulic fracturing effectiveness of the dense DFN configuration more than the sparse DFN configuration.

• The sparse DFN cases showed a flat microseismic distribution zone with few events while the dense DFN cases showed a complex microseismic map that indicated the intensive interaction between hydraulic fracture and the natural fractures.

- For all cases, the average DFN aperture increased only slightly during the injection while the average HF aperture increased significantly and was several times larger than the average DFN apertures. Relatively, the sparse DFN case showed a greater increase of average DFN aperture and average HF aperture than the dense DFN case for the same initial DFN aperture.

- This work suggests that fracture network connectivity plays a critical role in hydraulic fracturing effectiveness for unconventional shale developments, and fracture connectivity will play a significant role in optimizing treating pressures, the created microseismicity and corresponding SRV, and well production.

Author details

F. Zhang[*], N. Nagel, B. Lee and M. Sanchez-Nagel

*Address all correspondence to: fzhang@itascahouston.com

Itasca Houston, Inc., USA

References

[1] G. E. King, "Thirty years of gas shale fracturing: What have we learned?," in *SPE Annual Technical Conference and Exhibition*, Florence, Italy, 2010.

[2] C. Cipolla, M. Mack and S. Maxwell, "Reducing Exploration and Appraisal Risk in Low-Permeability Reservoirs Using Microseismic Fracture Mapping," in *Canadian Unconventional Resources and International Petroleum Conference*, Calgary, Alberta, Canada, 2010.

[3] N. R. Warpinski, "Integrating Microseismic Monitoring With Well Completions, Reservoir Behavior, and Rock Mechanics," in *SPE Tight Gas Completions Conference*, San Antonio, Texas, USA, 2009.

[4] S. F. Rogers, D. Elmo and W. S. Dershowitz, "Understanding Hydraulic Fracturing Geometry and Interactions in Pre-Conditioning through DFN Numerical Modeling," in *45th US Rock Mechanics / Geomechanics Symposium*, San Francisco, CA, 2011.

[5] W. S. Dershowitz, M. G. Cottrell, D. H. Lim and T. W. Doe, "A discrete fracture network approach for evaluation of hydraulic fracturing stimulation of naturally fractured reservoirs," in *44th US Rock Mechanics Symposium and 5th U.S.-Canada Rock Mechanics Symposium*, Salt Lake City, 2010.

[6] N. B. Nagel, M. A. Sanchez-Nagel, F. Zhang, X. Garcia and B. Lee, "Coupled Numerical Evaluations of the Geomechanical Interactions Between a Hydraulic Fracture

Stimulation and a Natural Fracture System in Shale Formations," *Rock Mechanics and Rock Engineering*, 2013.

[7] N. B. Nagel, X. Garcia, M. A. Sanchez-Nagel and B. Lee, "Understanding "SRV": A Numerical Investigation of "Wet" vs. "Dry" Microseismicity During Hydraulic Fracturing," in *SPE Annual Technical Conference and Exhibition*, San Antonio, Texas, USA, 2012.

[8] N. B. Nagel, M. A. Sanchez-Nagel, X. Garcia and B. Lee, "A Numerical Evaluation of the Geomechanical Interactions Between a Hydraulic Fracture Stimulation and a Natural Fracture System," in *46th US Rock Mechanics / Geomechanics Symposium*, Chicago, IL, 2012.

[9] N. Nagel, I. Gil, M. Sanchez-Nagel and B. Damjanac, "Simulating hydraulic fracturing in real fractured rock - overcoming the limits of pdeudo-3D models," in *SPE 140480 presented at the SPE Hydraulic Fracturing Technology Conference*, the Woodlands, TX, 2011.

[10] A. A. Savitski, M. Lin, A. Riahi, B. Damjanac and B. N. Nagel, "Explicit Modeling of Hydraulic Fracture Propagation in Fractured Shales," in *International Petroleum Technology Conference*, Beijing, China, 2013.

[11] ICG, *3DEC - Three-Dimensional Distinct Element Code, Version 4.2*, Minneapolis, MN: Itasca Consulting Group, Inc., 2007.